



Conversion of *Lavandula* Straw into High-Quality Solid Fuel: Effect of Hydrothermal Carbonization Conditions on Fuel Characteristics

Xin Li¹ · Sumeyra Seniha Baran¹ · François Orange² · Erik Bonjour³ · Patrick Jame³ · Gregory Verger-Dubois⁴ · Alice Mija⁵ · Claire Lomenech¹ · Pavel Kuzhir¹ · Charlotte Hurel¹ 

Received: 9 May 2022 / Accepted: 16 July 2022 / Published online: 26 July 2022
© The Author(s), under exclusive licence to Springer Science+Business Media, LLC, part of Springer Nature 2022

Abstract

Hydrochars obtained by hydrothermal carbonization (HTC) of *Lavandula* straws have been studied as an eco-friendly and economical valorization route of residual biomass from cosmetic industry into solid fuels. HTC process has been performed in a temperature range from 180 to 260 °C and retention time ranging from 1 to 20 h. The two key parameters (time and temperature) were normalized to severity factor (SF) ranging from 4.74 to 7.79, in order to compare the fuel characteristics of hydrochars according to the thermal treatment conditions. Proximate and ultimate analysis and microscopy and thermal analysis were used to characterize hydrochar surface, combustion behavior, and kinetics as a function of SF, and to compare them with those of the raw lavandin sample. Results showed that after HTC, hydrochar properties were close to sub-bituminous coal and lignite, and SF was a relevant optimization parameter for solid fuel application. In the case of *Lavandula*, SF = 6 was the optimal value for the HTC process. Nevertheless, in addition to SF, it is important to consider that HTC-temperature is a more influencing parameter than HTC-retention time for the fuel properties of the resulting hydrochars.

Keywords Biomass waste · Valorization · Severity factor · Lavandin · Cosmetic industry residues · Hydrochar

Introduction

France is a world leader in terms of perfume industry exportations. Perfume plant cultivation and transformation have been performed since the seventeenth century, mainly in the southeast region of France. Grasse (Alpes Maritimes, France) is the international capital of perfume, and concentrates most of the national industrial activity related to perfume and cosmetics. The *Lavandula* genus (lavender and lavandin), a native from the Mediterranean area, is cultivated

in Provence on around 20,000 ha of crops. Each year, more than 1000 tons of *Lavandula* essential oil is locally produced by water steam distillation. Lavandin essential oil production predominates over lavender due to its higher yield (100 kg/ha vs. 15 kg/ha for lavender) and its lower price, making it of interest for industry [1]. Nevertheless, due to the low concentration of essential oil in the crops, a huge amount of plant is distilled, and consequently a huge amount of solid residual biomass is generated (20,000 tons in France, representing 90% of the worldwide generation).

Given the current problems of reducing waste volume and greenhouse gas emissions, the environmental and ecological issues of straws from the perfume business are a major concern. Indeed, more than 40% of straws are discarded. Possible valorization routes of medicinal and aromatic plants biomass have been compiled in a recent review by Saha and Basak [2]. Among them, development of supplementary extractions to isolate molecules of pharmaceutical interest such as bioactive phytochemicals and bioactive phenolic antioxidants from the residual biomass was suggested to be more deeply investigated. Although this alternative seems very promising, it does not contribute to substantially decrease the residual biomass volume. Digestion of

✉ Charlotte Hurel
charlotte.hurel@univ-cotedazur.fr

¹ CNRS UMR 7010, Institut de Physique de Nice (INPHYNI), Université Côte d'Azur, Nice, France

² Centre Commun de Microscopie Appliquée (CCMA), Université Côte d'Azur, Nice, France

³ CNRS UMR 5280, Université Lyon 1, Institut Des Sciences Analytiques (ISA), Université de Lyon, Villeurbanne, France

⁴ JYTA, Carros, France

⁵ CNRS UMR 7272, Institut de Chimie de Nice (ICN), Université Côte d'Azur, Nice, France

residual biomass by microbes or bacteria to produce biogas or enzymes also attracted high attention since the production costs are low. Valorization of residual biomass as biofuels, biogas, biosorbents, biochars, and biopesticides was also investigated, as well as reuse of residual biomass as soil amendment, organic mulch, and animal feed [2].

Concerning *Lavandula* straw (LS) valorization, utilization as feedstock for producing high-added value compounds (antioxidants, aroma), fungal oxidative enzymes to improve decomposition of lignocellulose into biofuel [3], and conversion into mycelium-based biomaterials [4] have been proposed as interesting issues. The use of LS as a co-composting material mixed with cattle manure and barley straw has also been recently investigated and results showed that organic matter degradation was accelerated in the presence of LS despite some negative aspects such as increased C/N ratio and a decrease in germination index which have been pointed out [5]. To our knowledge, LS is for now in majority pyrolyzed in treatment units far away from their production site. LS valorization as solid fuel has never been investigated, whereas many kinds of biomass have already been investigated as solid fuel: wood and woody biomass, agricultural biomass, aquatic biomass, human and animal biowaste, industrial biomass—alone or mixed with other varieties of biomass [6].

The main processes for the production of solid fuel from biomass include pyrolysis, torrefaction, and hydrothermal carbonization. These thermal conversion techniques result in carbon-rich materials whose properties depend on the type of process and the reaction parameters. Pyrolysis involves a thermal treatment at elevated temperature (300–650 °C) under inert atmosphere; in the torrefaction process, biomass is heated in the absence of oxygen at 200–300 °C for less than 1 h at ambient pressure, whereas HTC is performed in a closed vessel, under self-generated pressure (2–10 MPa) obtained by heating under moderate temperature (180–250 °C) for several hours [7, 8]. Many practical and economical advantages of HTC process can be enumerated, compared to pyrolysis and torrefaction, making this process a promising valorization route of biomass into solid fuel. Indeed, wet samples can directly be processed by HTC, and to a lesser extent by torrefaction when the moisture content is lower than 15%, whereas a costly drying step is required for pyrolysis [9]. HTC results in a solid fuel (hydrochar) with properties comparable to the solid product obtained by torrefaction, such as mass yield and higher heating value (HHV). However, the temperature applied during HTC is lower than for torrefaction for the same mass yield [9]. Compared to pyrolysis where the presence of water decelerates the process, the presence of water during HTC results in an increase of the rate of carbonization and a higher yield compared to pyrolysis process applied to samples without water [6]. The presence

of water enhances biomass decomposition by hydrolysis reactions and results in a lower ash content by leaching [9]. HTC results in a more severe decomposition of biomass and a higher increase of the HHV for a given mass of raw biomass than torrefaction [7].

On an economical and technical point of view, when scaling up HTC process, solutions have to be found considering the complexity of the process (compared for example with torrefaction), the high pressure during HTC (in order to overcome the use of expensive, very resistant materials), and the energy required [8, 10]. A drying step after production of the obtained hydrochar has also to be considered for an industrial process [8]. The batch process is the more commonly considered at scales ranging from bench level to pilot scale giving the ease of implementation and scale-up, but one of its main drawbacks is the large energy consumption. Semi-continuous processes have been proposed as fixed-bed, flow-through reactors, in which hot water is pumped through the reactor which retains biomass. They have proven to be cost-effective at small industrial scale with varied feedstocks. A continuous process is generally selected at large scale for economic reasons because of the lower energy associated with reactors with high solid contents and constant temperatures [10].

Factors affecting HTC process are (i) temperature, (ii) biomass composition, (iii) retention time (i.e., duration of thermal treatment), and (iv) water to biomass ratio. Among these factors, temperature and retention time have been pointed out to be probably the key parameter. When high temperatures were applied, solid fuel quantity was low but it presented high carbon content and elevated HHV. In contrast, when low temperatures were applied, the solid fuel production was higher due to an incomplete decomposition of cellulose and hemicellulose. Higher retention times also resulted in a better solid yield, as well as high values of autogenerated pressure [6]. These two variable parameters are usually reduced into one, called the severity factor (SF) initially proposed by Overend and Chornet (1987) [11] to describe the impact of liquid hot water treatments on lignocellulosic components. Depending on retention time and temperature during HTC process, SF generally ranges from 4 to 8 [12]. This range of SF values can be attained either through a combination of a high temperature/short retention time; or moderate temperature/high retention time, or moderate temperature/moderate retention time. Since a same SF can be reached by either a combination of short retention time/high temperature or long retention time/low temperature, there is a loss of interpretation especially regarding the weight of each parameter (retention time/temperature) when using SF. Nevertheless, for practical reasons, the reduction of the HTC conditions to one degree of freedom makes easier the comparison of hydrochar properties, and is generally used.

Biomass valorization as solid fuel through HTC depends on the composition of the original biomass. During HTC of lignocellulosic biomass, which is mainly composed of cellulose, hemicellulose, and lignin [7], reaction paths result in dehydration, decarboxylation, aromatization, hydrolysis, and condensation of these three different fractions, but the exact mechanisms are still under elucidation [13]. A higher lignin content in the samples resulted in a higher yield of the production of solid fuel whereas a higher content of cellulose and hemicellulose increased the yield of the liquid phase [6]. Among the different sources of biomass, the fuel properties of hydrochars obtained from agricultural waste are noticeably improved compared to those of the agricultural waste before HTC treatment, with combustion properties similar of those of brown coal [14]. As an example, the HHV of corn silage is improved from 19.6 to 26.6 MJ·kg⁻¹ while the HHV of dough residues is improved from 17.8 to 28.3 MJ·kg⁻¹ [14]. The ignition temperature, which is a key parameter when considering safety storage of fuels, also increases after HTC treatment of agricultural residues, as well as the coalification degree and the fixed carbon content, while the quantity of volatile matter decreases [15, 16].

The objective of this work is to evaluate the potential of HTC as an adapted conversion route from technical, economic, and environmental perspectives for LS valorization as solid fuel, which has never been investigated before. The benefits of HTC treatment are nevertheless strongly dependent on the biomass; therefore, a complete study of the physico-chemical and combustion characteristics of LS hydrochars has to be firstly performed. Then, to evaluate the relevance of using SF as unique parameter to determine the optimal HTC conditions for solid fuel production, an investigation on the weight of each parameter—SF, retention time, and temperature—is needed. These are the aims of this work. For that, HTC conditions were investigated under a constant water to biomass ratio and variables retention time (from 1 to 20 h) and temperatures (from 180 to 260 °C) in order to get SF ranging from 4.74 to 7.79. Proximate and ultimate analysis, scanning electron microscopy (SEM), and attenuated total reflectance infrared spectroscopy (ATR-FTIR) were performed on lavandin sample and hydrochars for characterization. Then, combustion behavior and combustion kinetics were studied with the help of thermogravimetric analysis (TGA), in order to evaluate the influence of each parameter, severity factor, retention time, and temperature, on the properties of hydrochars, in the context of their utilization as solid fuel.

Materials and Methods

Lavandin Sample and Hydrochar Preparation

Air-dried lavandin (L) samples were collected in the Alpes-Maritimes (GPS coordinates: 43.765533; 7.345123), France. They were ground using a domestic

blender then dried in an oven at 105 °C until a constant mass was reached (approximately 24 h). A Fritsch Analysette vibrating sieve equipped with several sieves of different sizes was used to discriminate the ground dried particles by their size. The size fraction providing the most abundant volume of sample was 125–500 µm. It has been shown that hydrochars produced from samples with particle size under 250 µm had a higher HHV and the carbon content was higher in the solid phase [17]. Hence, in order to get hydrochars with high HHV and to valorize a large amount of biomass, L hydrochars were produced from 125–500-µm particles.

The hydrothermal carbonization (HTC) of the L was performed in a 600-mL sealed reactor (Series 4560 Mini Reactors, Parr Instrument Company) equipped with stainless steel vessel, polytetrafluoroethylene (PTFE) flat gasket, and mechanical stirring device (Fig. S1). A constant initial solid/liquid ratio (S:L = 1:5) was chosen for all HTC experiments. For that, 20 g of L and 100 mL of deionized water were inserted in the reactor. This ratio has been fixed to 1:5 because it corresponded to the minimum amount of water to be added inside the reactor that allowed the stirrer to constantly homogenize the mixture, and allowed a sufficient humidity for an efficient and homogeneous heat transfer during HTC. In addition, it has been demonstrated that when S:L ratio was greater than 1:5, a decrease in hydrochar yield due to dissolved biomass components in the liquid fraction could occur [13]. The reactor was wrapped in an electric furnace, heated to the desired temperature (180–260 °C) with a heating ramp of 6.8 °C/min (starting from 25 °C; Fig. S2), and maintained at the set point temperature for several hours (1–20 h). When the desired retention time was reached, the reactor was removed from the electric furnace to naturally cool at room temperature. Cooling occurred with a ramp of 1.6 °C/min (Fig. S2). HTC reaction occurred under self-generated pressure. The slurry after the HTC reaction was filtered by pre-weighed filter paper; the solid phase was separated and dried in an oven at 105 °C until a constant mass was reached and manually ground. Table 1 shows details of sample preparation during HTC. Raw L and its corresponding hydrochars were abbreviated as L and LHx-y, respectively. The retention time (in hours) and temperature (in °C) were represented by *x* and *y*, respectively. These peculiar combinations of retention time and temperature have been chosen in order to discuss about the influence of retention time on one hand and temperature on the other hand on hydrochar properties and to conclude about the relevance of using SF as an optimization parameter for fuel application.

HTC treatments use water as reaction medium for biomass pretreatment. Temperature and retention time are the most important variables affecting the efficacy of pretreatment.

Table 1 Details of sample preparation during HTC

Sample ID	Retention time (h)	Temperature (°C)	SF	S:L
L	0	NA	NA	NA
LH1-220	1	220	5.31	1:5
LH2-220	2	220	5.61	1:5
LH4-220	4	220	5.91	1:5
LH8-220	8	220	6.21	1:5
LH20-220	20	220	6.61	1:5
LH4-180	4	180	4.74	1:5
LH4-200	4	200	5.32	1:5
LH4-240	4	240	6.50	1:5
LH20-200	20	200	6.02	1:5
LH20-240	20	240	7.20	1:5
LH20-260	20	260	7.79	1:5

The combination of these two factors into a single one allows comparison of the experimental results. Overend and Chor-net (1987) proposed the reaction ordinate concept (R_0) to combine time and temperature parameters. In this concept, the assumption is done that (i) the reaction occurs in a single step, is irreversible, and its overall kinetics follow a first-law concentration dependence; (ii) the rate constant has an Arrhenius-type dependence on temperature [11]. The reaction ordinate is expressed by the following equation:

$$R_0 = t \times \exp\left(\frac{T - 100}{14.75}\right) \quad (1)$$

With R_0 being the reaction ordinate (min), t being the retention time (min), T the temperature (°C), 100 °C is the reference temperature, and 14.75 °C is the temperature increase which has an exponential relation with reaction order to produce the same changes in the hydrochar [18]. The severity factor (SF), corresponding to $\log R_0$, is generally used to evaluate the efficiency of the process.

Proximate Analysis

The proximate analysis including moisture (M), ash (Ash), and volatile matter (VM) contents of L and hydrochars was determined using a thermogravimetric analyzer (Mettler Toledo TGA2 Star System), based on American Society for Testing and Materials (ASTM) E871-82 [19], ASTM E1755-01 [20], and ASTM E872-82 [21] methods, respectively. The fixed carbon (FC) content percentage was calculated as:

$$FC(\%wt) = 100 - M(\%wt) - VM(\%wt) - Ash(\%wt) \quad (2)$$

Depending on their fuel ratio (FR), the hydrochars can be ranked as alternative coal fuels. A low fuel ratio suggests

that the fuel easily ignites due to its high volatile matter content. Hence, an increased fuel ratio suggests that the fixed carbon content of the fuel is higher than its volatile matter content, providing better fuel properties. Hydrochar yield (HY) allows estimating how interesting the chosen biomass is, regarding the quantity of produced hydrochar from the initial biomass.

FR and HY were calculated as follows:

$$FR = \frac{FC(\%wt)}{VM(\%wt)} \quad (3)$$

$$HY(\%) = \frac{\text{dried hydrochar mass}}{\text{dried biomass mass}} \times 100. \quad (4)$$

Elemental Analysis

C and H measurements were performed on a C/H elemental micro-analyzer (ISA, CNRS, Villeurbanne). About 1.5 mg of sample weighted in silver cups was dropped into a flow of 50 mL min⁻¹ of pure O₂ into a unit combustion hold at 1050 °C and half-filled with CuO. C and H were transformed into CO₂ and water H₂O, respectively, prior to be measured using a CO₂/H₂O non-dispersive infrared detector. The precision has been evaluated at ±0.30% for C and H.

N analysis was taken into account using a nitrogen elemental micro-analyzer (ISA, CNRS Villeurbanne). The sample weighted in silver cup falls in a similar unit combustion previously described where N has been turned into nitrogen oxide in a flow of He and O₂. The gasses pass through a copper wire tube held at 450 °C where nitrogen oxide was reduced in N₂ followed by a CO₂/H₂O trap. The quantification of the resulting N₂ has been done on a TCD (thermal conductivity detector). Precision has been established < 0.20%.

S determination has been performed using a C/S SC144 analyzer (LECO, St Joseph, USA). About 10 mg of samples has been introduced into a horizontal combustion unit maintained at 1350 °C where C and S are turned into CO₂ and SO₂ prior to quantifying using CO₂ and SO₂ non-dispersive infrared cells. Precision on S analysis was evaluated at 0.10%.

Calorific values (HHV) were calculated from elemental analysis and ash content according to Channiwala et al. (2002) [22]. The validity of this correlation has been established for fuels ranging from gaseous, liquid, coals, biomass material, and char to residue-derived fuels having a wide range of elemental composition (C: 0–92.25%; H: 0.43–25.15%; O: 0–50%; N: 0–5.6%; S: 0–94.08%, Ash: 0–71.4%). The versatility of this correlation has been

demonstrated through a bias error of 0% and an average absolute error of 1.45%.

$$HHV = 0.349C + 1.1783H + 0.1005S - 0.1034O - 0.0015N - 0.0211Ash \quad (5)$$

with HHV in (MJ kg^{-1}); C , H , S , O , N , and Ash in (% wt). According to Eq. 5, the high HHV value is correlated to high C , S , and H contents and low O , N , and Ash contents.

Energy densification ratio (EDR) of hydrochars was calculated from HHV values of hydrochar and biomass as follows:

$$EDR = \frac{HHV_{hydrochar}}{HHV_{biomass}} \quad (6)$$

Energy yield (%) (EY) was calculated from EDR and HY as follows:

$$EY = EDR \times HY \quad (7)$$

Extractives and Klason Lignin Determination

Extractives in L, LH4-220, LH20-220, and LH-20–240 were determined according to [23]. Ethanol was used as solvent. Seven grams of moisture-free biomass was weighed and placed in a thimble (filter paper). The thimble was placed in a 100-mL Soxhlet apparatus. Several boiling chips were placed in a 250-mL flask. The Soxhlet and flask were connected. In total, 160 mL of 190 proof ethanol (95% ethanol) was added to Soxhlet. The Soxhlet and condenser were connected. The system was heated at reflux for 6 h. After 6 h, the thimble was washed with 50 mL of ethanol and filtrated. Then, the thimble and sample were dried at room temperature. The dried extractive-free sample was weighed. Extractive percentage was calculated by mass loss between the moisture-free sample and extractive-free sample.

Klason lignin in L, LH4-220, LH20-220, and LH-20–240 was determined according to [24]. The 0.5 g extractives – free sample was weighed and placed in a flask. A total of 7.5 mL sulfuric acid (H_2SO_4) (72%) solution was added to the flask. The flask was held in a water bath for 2 h at 20 °C. After 2 h, 280 mL distilled water and magnetic stirring bar were added to the flask. The flask and condenser were connected. Flask was boiled for 4 h at 100 °C on a magnetic stirrer. After 4 h, the sample was washed until sulfate ion removal and filtrated. Then, the sample was dried at room temperature. The dried sample was weighed. Klason lignin percentage was calculated using mass loss between extractives-free sample and klason lignin-free sample.

SEM, ATR-FTIR

Surface morphologies of L and hydrochars were investigated with scanning electron microscopy (SEM). Observations were performed with a Tescan Vega3 SEM, using secondary electron with a 5-kV voltage and in high vacuum mode with various magnifications. Particle size distribution was determined from SEM images of each sample, using ImageJ free open-source software [25]. From each sample picture, at least 30 to 50 particles with clear and easily distinguishable outlines were selected for size measurement with ImageJ software.

Fourier-transform infrared (FT-IR) spectrometer (Nicolet iS50 FT-IR spectrometer with a GladiATR single diamond attenuated total reflectance system (PIKE Technologies, Inc.)) was used to ascertain the change of functional groups and chemical bonds on the surfaces of L and its hydrochars. For each sample, 32 scans were performed, in the wavenumber range between 400 and 4000 cm^{-1} with a resolution of 4 cm^{-1} .

Combustion Behavior of Lavandin and Hydrochar Samples

Thermogravimetric analysis (TGA) of L and hydrochars was performed by Mettler Toledo TGA2 (operated with Star software) under constant air flow (150 mL min^{-1}) at temperatures between 25 and 1000 °C with a constant heating rate (10 °C min^{-1}), in order to evaluate the combustion behavior of the samples. A mass of approximately 10 mg was inserted into TGA crucibles, and a heating rate of 10 °C min^{-1} was applied. These conditions were satisfactory to limit the possible heat and mass transfers during TGA [26]. Ignition (T_i) and burnout (T_b) temperatures were determined according to the intersection method and conversion method, respectively, as suggested by Lu and Chen [27]. T_i corresponds to the minimum temperature at which fuel spontaneously ignites without external source of ignition, and T_b corresponds to the temperature at which 99% of the initial biomass is consumed. Both parameters are crucial for evaluating fuel properties and conditions for safe storage and transportation.

Combustibility index (S) reflects the ignition, combustion, and burnout properties of fuel. This index can be calculated from information extracted from the DTG curves as:

$$S = \frac{\left(\frac{dw}{dt}\right)_{max} \left(\frac{dw}{dt}\right)_{mean}}{T_b \times T_i^2} \quad (8)$$

where $\left(\frac{dw}{dt}\right)_{max}$ and $\left(\frac{dw}{dt}\right)_{mean}$ were the maximum mass loss rate ($\% \text{ min}^{-1}$) and the average loss rate ($\% \text{ min}^{-1}$) from

DTG curves, respectively, and T_b and T_i the burnout and ignition temperatures (°C) respectively.

The larger the value of S , the higher combustion activity is. It is generally admitted that S higher than $2 \times 10^{-7} \text{ g}^2 \text{ min}^{-2} \text{ }^\circ\text{C}^{-3}$ corresponded to interesting material for fuel purposes [28].

Calculation of Kinetic Parameters [29]

To determine the kinetics parameters related to thermogravimetric experiments, it is generally assumed that the reaction rate of such processes can be kinetically described by Arrhenius integral approach. Coats and Redfern [30] proposed a determination method of activation energy and preexponential factor based on the definition of a dimensionless thermal conversion factor (α): $\alpha = \frac{(m_i - m)}{(m_i - m_f)}$, where m_i, m , and m_f are initial, instantaneous, and final mass of a sample, respectively. This model assumes that only a single reaction occurs while a sample undergoes a certain temperature rise at a steady heating rate (β). Coats-Redfern model (CR model) has been widely used in the literature to determine activation energy (E) and pre-exponential factor (A) of combustion reactions at a constant β [31, 32]. CR model has been applied to thermogravimetric data. In this model, the mass change vs temperature is described as:

$$\frac{d\alpha}{dT} = \frac{A}{\beta} e^{\left(-\frac{E}{RT}\right)} (1 - \alpha)^n \tag{9}$$

where A is the pre-exponential factor (min^{-1}), E is the activation energy (J mol^{-1}), R is the gas constant ($8.314 \text{ J mol}^{-1} \text{ K}^{-1}$), T is the temperature (K), α the thermal conversion factor of the sample at a given time (t) calculated from TG/DTG curves, and n is the order of reaction.

Integral of Eq. 9 gives:

$$\int_0^\alpha \frac{d\alpha}{(1 - \alpha)^n} = \int_{T_0}^T \frac{A}{\beta} e^{\left(-\frac{E}{RT}\right)} dT \tag{10}$$

Considering the approximation proposed by Coats and Redfern integration of Eq. 10 gives [30]:

$$\ln \left[\frac{-\ln(1-\alpha)}{T^2} \right] = \ln \left(\frac{AR}{\beta E} \left(1 - \frac{2RT}{E} \right) \right) - \frac{E}{RT} \text{ for first - order reaction } (n = 1) \tag{11}$$

Or

$$\ln \left[\frac{1-(1-\alpha)^{1-n}}{(1-n)T^2} \right] = \ln \left(\frac{AR}{\beta E} \left(1 - \frac{2RT}{E} \right) \right) - \frac{E}{RT} \text{ for order } n \neq 1 \tag{12}$$

Considering that $E > 10 \text{ kJ mol}^{-1}$ and $T < 500 \text{ K}$, $\frac{RT}{E} \ll 1$, Eq. 11 and Eq. 12 are simplified as:

$$\ln \left[\frac{-\ln(1-\alpha)}{T^2} \right] = \ln \frac{AR}{\beta E} - \frac{E}{RT} \text{ for order } 1 \tag{13}$$

$$\ln \left[\frac{1-(1-\alpha)^{1-n}}{(1-n)T^2} \right] = \ln \frac{AR}{\beta E} - \frac{E}{RT} \text{ for order } \neq 1 \tag{14}$$

The linear regression equation of plot of $\ln \left[\frac{-\ln(1-\alpha)}{T^2} \right]$ or $\ln \left[\frac{1-(1-\alpha)^{1-n}}{(1-n)T^2} \right]$ vs $\frac{1}{T}$ allows the determination of activation energy (E) and pre-exponential factor (A) (Table S1).

Results and Discussion

Proximate and Elemental Analyses of L and Hydrochars

Table 2 presents proximate and elemental analyses of L and hydrochars. M content of L was initially low ($< 3\%$ wt) compared to other biomass (eucalyptus, olive stones, triticale, cork, etc.) [33]. After HTC treatment, M content decreased below 1%. For hydrochars obtained at $220 \text{ }^\circ\text{C}$, the influence of retention time (from 1 to 20 h) on M content can be discussed. M decreased as retention time increased from 1 to 20 h, the minimum value for M being 0.4% for LH20-220. For hydrochars obtained at retention time of 4 h and temperature ranging from 180 to $240 \text{ }^\circ\text{C}$, M content decreased as temperature increased and the minimum M content was 0.39% for LH4-240. A 50% decrease of M content was observed between LH4-200 and LH4-220, indicating that a temperature variation of $20 \text{ }^\circ\text{C}$ strongly reduced the M content. Such a decrease was not noticeable when the retention time was increased from 1 to 20 h at $220 \text{ }^\circ\text{C}$. For hydrochars obtained at retention time of 20 h, and temperature ranging from 200 to $260 \text{ }^\circ\text{C}$, the minimum M content was 0.33% for LH20-260. The minimum M content was obtained for hydrochars prepared under HTC conditions corresponding to $\text{SF} > 6$. Hence, HTC conditions corresponding to $\text{SF} > 6$ allowed getting hydrochars with the lowest M content. Nevertheless, between retention time and temperature, which are the two parameters used for SF calculation, temperature seems to be the more influencing one on M content.

At HTC-temperature of $220 \text{ }^\circ\text{C}$, VM decreased from 81 to 61% (LH20-220) in L and hydrochars respectively, depending on HTC-retention time increase. For hydrochars obtained at HTC-retention time of 4 h and HTC-temperature ranging from 180 to $240 \text{ }^\circ\text{C}$, a 10% decrease of VM was obtained. The same VM decrease was obtained when HTC-retention time was long (20 h) and the temperature ranged from 200 to $260 \text{ }^\circ\text{C}$. The lowest VM contents were obtained for LH20-260, LH20-240, and LH20-220 corresponding to hydrochars obtained under HTC conditions corresponding to $\text{SF} > 6$. Temperature seemed to be the most influencing parameter for VM content reduction.

The trend for FC content was opposite to the one described for VM content. For hydrochars obtained at HTC-temperature of $220 \text{ }^\circ\text{C}$, FC increased from 22 to 34%, this

Table 2 Proximate and ultimate analyses of lavender sample and hydrochars

L	LH1-220	LH2-220	LH4-220	LH8-220	LH20-220	LH4-180	LH4-200	LH4-240	LH20-200	LH20-240	LH20-260
SF	NA	5.31	5.61	5.91	6.21	4.74	5.32	6.50	6.02	7.20	7.79
Moisture (%)	2.93	0.68	0.65	0.51	0.42	1.21	1.06	0.39	0.65	0.39	0.33
Volatile matter (%)	80.89	72.66	70.28	67.08	63.6	70.19	74.96	61.65	65.54	58.43	54.91
Fixed carbon (%)	8.55	21.86	24.07	27.77	31.2	23.25	19.83	33.22	28.41	35.76	37.8
Ash (%)	7.63	4.8	5.0	4.64	4.78	5.35	4.15	4.74	5.4	5.42	6.96
Fuel ratio	0.11	0.30	0.34	0.41	0.49	0.33	0.26	0.54	0.43	0.61	0.69
C (%)	50.77	60.42	61.54	64.98	67.24	58.79	61.35	69.65	65.31	71.94	71.59
H (%)	6.9	6.81	6.31	6.27	6.28	6.48	6.21	6.75	6.82	6.65	6.04
N (%)	1.28	1.09	1.18	1.31	1.44	1.29	1.24	1.53	1.46	1.69	1.77
O (%)	41.05	31.68	30.97	27.44	25.04	33.44	31.2	22.07	26.41	19.72	20.6
S (%)	0.33	<0.3	<0.3	<0.3	<0.3	<0.3	<0.3	<0.3	<0.3	<0.3	<0.3
Extractives (%)	5.5			14.2						14.7	
Klason lignin (%)	33.2			46.7						78.6	
HHV (MJ/kg)	21.43	25.72	25.59	27.12	28.16	24.57	25.40	29.86	27.97	30.77	29.81
Energy densification	NA	1.2	1.2	1.3	1.3	1.2	1.2	1.4	1.3	1.4	1.4
Energy yield (%)	NA	65.15	61.05	60.31	55.59	68.26	64	57.75	66.51	58.11	53.63
Hydrochar yield (%)	NA	54.27	51.12	47.66	42.3	59.54	53.99	41.44	50.96	40.47	38.56

content being much higher than *FC* content of initial biomass content (8.5%). When HTC-retention time was 4 h and HTC-temperature ranged from 180 to 240 °C, the maximum *FC* content was reached for LH4-240 (33%), corresponding to SF=6.5. A slightly higher *FC* content was obtained for LH20-260 (38%), when HTC-retention time was 20 h and the HTC-temperature ranged from 200 to 260 °C. Hence, hydrochars prepared under SF conditions superior to 6 provided the highest *FC* contents. Compared to retention time, temperature seemed to be the most influencing parameter for *FC* content increase.

Compensation of *VM* decrease by *FC* increase is represented by *FR*. High *FR* value is required for solid fuel application since it points out better fuel properties with lower gas emission and efficient combustion. *FR* was 0.11 for L and it ranged from 0.3 to 0.69 for hydrochars. These *FR* values were on the same order of magnitude as for rice and coconut husk hydrochars [34], and were higher than *FR* values of hydrochars obtained from filamentous algae (*Hippeastrum reticulatum*) and microalgae (*Chlorella vulgaris*), respectively [35]. Evolution of *FR* depending on SF is presented on Fig. 1a, and is compared to *FR* from Liu et al. [28] for coconut fiber and eucalyptus leaf hydrochars obtained with the

same S:L conditions as the one used in this study. *FR* were in the same order of magnitude for lavandin hydrochars, coconut fiber hydrochars, and eucalyptus leaf hydrochars as well as SF. *FR* linearly increased with SF for the three kinds of hydrochars. The growth rate was the same for lavandin and coconut fiber hydrochars, and it was slightly lower for eucalyptus leaves. Evolution of fuel ratio indicated that at the highest SF values, *FC* content was the highest and *VM* content was the lowest. For hydrochars, sample LH20-260 presented the highest *FR*, compared to other hydrochars. The highest *FR* were obtained for LH20-220, LH4-240, LH20-240, and LH20-260, corresponding to hydrochars obtained under HTC conditions with SF > 6.

Ash content in L was around 7.6% and it was lower for all hydrochars (around 5%). The decrease in Ash content of LH compared to L is due to the release of inorganic elements into the liquid fraction that enhance the biomass conversion. For hydrochars obtained under HTC-temperature of 220 °C and retention times ranging from 1 to 20 h, no significant change in Ash content can be noticed. The same observation can be done about hydrochars obtained at HTC-retention time of 4 h and 20 h and temperature ranging from 180 to 240 °C and 200 to 260 °C, respectively, except for Ash

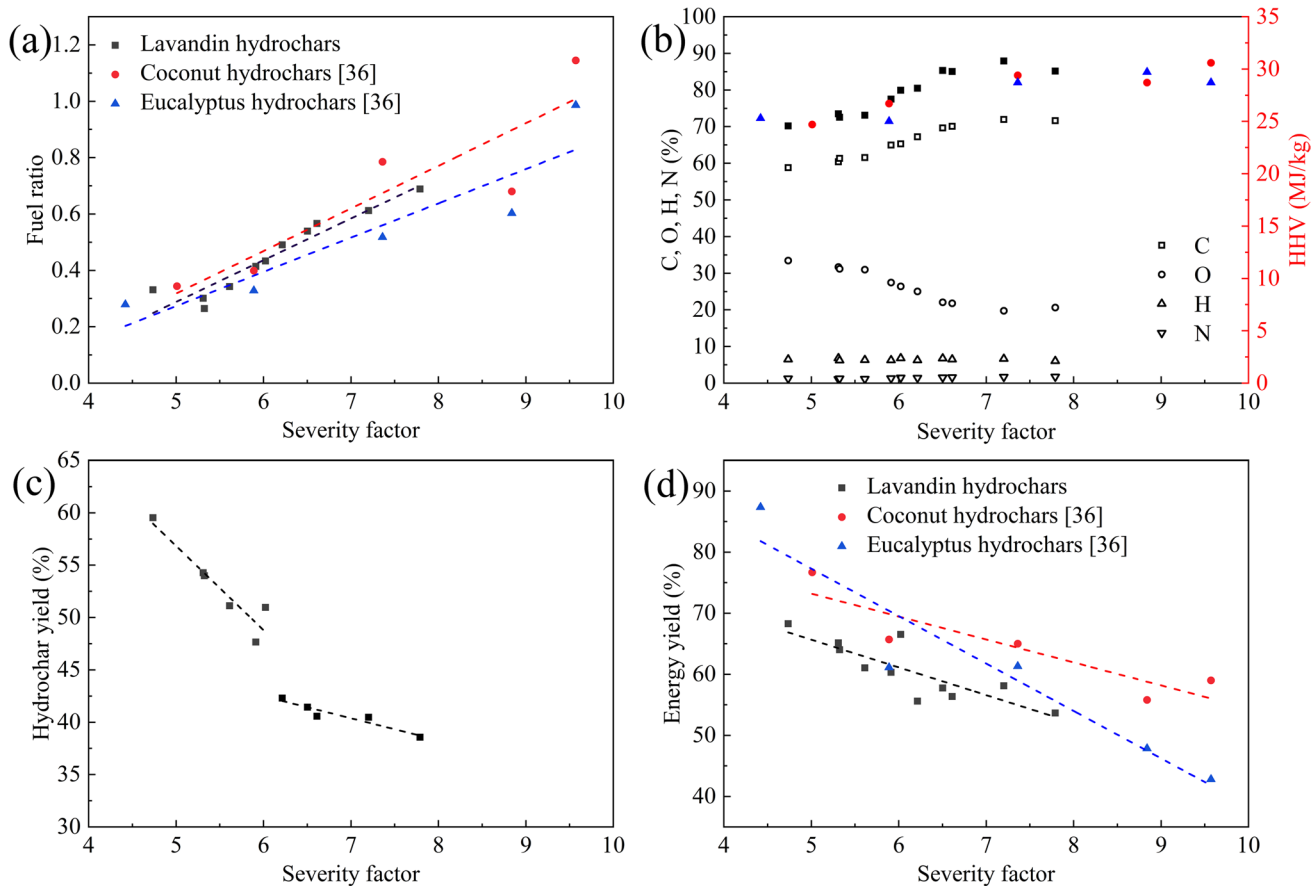


Fig. 1 Evolution of **a** fuel ratio; **b** HHV, %C, %O, %H, %N; **c** hydrochar yield; **d** energy yield as a function of severity factor

content of LH20-260 that is much higher than the others (7%). This high *Ash* content under severe HTC conditions has been reported previously [34]. According to the authors, it could be due either to a dissolution and decomposition at a rapid rate of other components or to readsorption of some inorganic components on the surface of hydrochar. Hence, regarding *Ash* content, high SF conditions could negatively influence hydrochar properties for fuel applications.

From ultimate analysis, C content in hydrochars increased as SF increased, while O content decreased as SF increased. N and H variations were less noticeable (Fig. 1b), and S content was negligible (inferior to detection limit) both for LS and hydrochars.

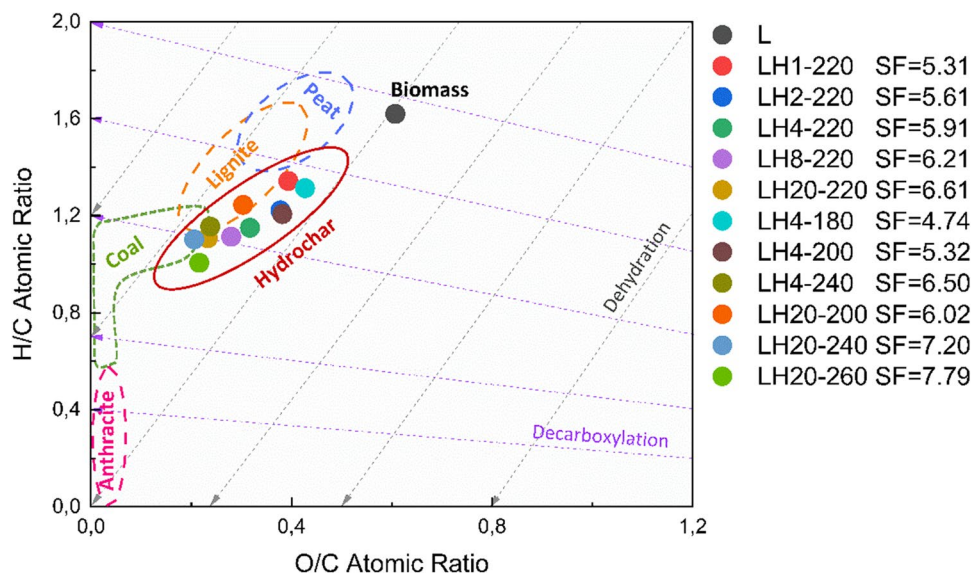
Extractives and Klason lignin contents were reported for L, LH4-220, LH20-220, and LH20-240. Compared to L sample, the amount of extractives and Klason lignin was increased in hydrochars.

Calculated *HHV* ranged from 21.43 MJ kg⁻¹ for L to 30.77 MJ kg⁻¹ for hydrochars. These *HHV* were in the same order of magnitude than hydrochars from miscanthus, eucalyptus bark, empty fruit brunches, pine wood meal, lignocellulosic biomass, eucalyptus leaves, and coconut fibers [6, 36]. Figure 1b presents evolution of *HHV* versus SF for lavandin hydrochars, and coconut fiber and eucalyptus leaf hydrochars from Liu et al. [28], for comparison. *HHV* obtained at different SF for different kind of biomass and the same S:L initial condition were of the same order of magnitude and ranged from 25 to 30 MJ kg⁻¹. The trend of *HHV* as a function of SF was directly correlated to the trend of C content in hydrochar and inversely correlated to the trend of O content. From SF 4 to 5, *HHV* remained constant as well as C and O contents. Considering C, H, O, N, and *Ash* compositions from Table 2, hydrochars prepared under HTC conditions corresponding to SF 4 to 5 presented similar compositions, and consequently presented similar *HHV*. For HTC conditions corresponding to SF 5 to 6, *HHV* increased from 25 to 30 MJ kg⁻¹, indicating that HTC conditions were significantly different to provide hydrochars with different compositions of C, H, O, N, and *Ash*. For HTC conditions corresponding to SF 6, *HHV* reached a plateau and remained constant whatever the SF value, indicating that above SF6 hydrochars presented similar compositions in terms of C, H, N O, and *Ash*. This described trend was the same for coconut and eucalyptus hydrochars, with an increase of *HHV* for SF from 5 to 6, then above SF 6 *HHV* value did not change significantly and remained stable. In conclusion, regarding *HHV* value, optimal HTC condition could be proposed to provide hydrochars with interesting calorific values. *EDR* ranged from 1.2 to 1.4; the highest value was obtained for hydrochars obtained at SF > 6.5. Figure 1c presents evolution of *HY* as a function of SF. Two distinct segments arose: the first one concerned SF

from 4 to 6 where *HY* strongly decreased with a slope near to 8%/SF unit; the second segment concerned SF above 6, where *HY* decrease was slighter with a slope near 2%/SF unit. Regarding optimal *HY*, SF around 6 seemed to be a good compromise for solid fuel application. Evolution of *EY* as a function of SF is presented in Fig. 1d. In the range of SF studied, *EY* of lavandin hydrochars decreased from 68 to 53%, and the maximum value for *EY* corresponded to the sample obtained at the lowest SF value. Compared with *EY* for coconut fiber and eucalyptus leaf hydrochars [28], lavandin, coconut fiber, and eucalyptus hydrochars had *EY* in the same order of magnitude and depicted a linear decrease trend as SF increased and the rates of decay were similar. The rate of decay was similar for lavandin and coconut fiber hydrochars, whereas it was higher for eucalyptus leaf hydrochars, indicating that the latter presented a less interesting *EY* compared to lavandin and coconut fibers for solid fuel application.

The atomic ratios H/C and O/C of lavandin and hydrochars are presented in Fig. 2, as the van Krevelen diagram, in order to compare biomass and hydrochars with fossil fuels. Pathways for dehydration and decarboxylation are also illustrated. L has high H/C and O/C ratios indicating that this biomass could not be used efficiently as solid fuel. On the contrary, hydrochars showed a wide range of quality ranging from sub-bituminous coal to lignite. HTC process allowed dehydration along with decarboxylation, with different extent depending on treatment conditions. When hydrochars were obtained at SF superior to 6.5, H/C and O/C ratios were close to coal. When hydrochars were obtained at SF < 6.5, H/C and O/C ratios were close to lignite. Demethylation should depict a decrease of H/C atomic ratio with an increase of O/C atomic ratio. This trend was not observed for hydrochars. The effect of HTC-retention time and HTC-temperature on H/C and O/C ratio can be discussed. For hydrochars obtained at HTC-temperature of 220 °C, the increase of retention time from 1 to 20 h enhanced the dehydration and the decarboxylation process. When HTC-retention time was 4 h and HTC-temperature ranged from 180 to 240 °C, hydrochar quality was close to lignite except for LH4-240 which was close to both sub-bituminous coal and lignite. When HTC-retention time was 20 h and HTC-temperature ranged from 200 to 260 °C, hydrochar quality was close to sub-bituminous coal except for LH20-200, which was close to lignite. From the Van Krevelen diagram, it can be concluded that hydrochars obtained for HTC conditions corresponding to SF superior to 6.5 presented properties close to sub-bituminous coal. Regarding HTC-temperature and HTC-retention, it can be concluded that it is preferable to use a combination of high temperature/short retention time to reach SF close to 6.5. This confirms that temperature is the most influencing factor on hydrochar properties.

Fig. 2 van Krevelen diagram for lavandin biomass and hydrochars



SEM and ATR-FTIR

The surface morphologies of L and its corresponding hydrochars are visualized in Figs. S3 and S4. Because of using the blender to crush the L, broken branches and broken flowers can be seen from Fig. S3 (a). In Fig. S4 (a), L showed fibrous structure with a smooth surface which is the typical structure of herbaceous biomass) [37].

After the HTC process, each hydrochar had different levels of decomposition. The flower part completely disappeared after the HTC process. Corresponding to different experimental conditions, a great quantity of large-sized fibrous structures in LH1-220, LH2-220, LH4-220, LH4-180, and LH4-200 were preserved (Fig. S3 (b, c, d, g, h)), whose SF were less than 6. Further hydrolysis of cellulose or hemicellulose and partial hydrolysis of lignin, with the increase in SF, LH8-220, LH20-220, LH4-240, and LH20-200 samples, was dominated by heterogeneous fragments so that only a few fibrous structures were observable as shown in Fig. S3 (e, f, i, g) [38]. When the SF were superior to 7, which represented the hydrochars LH20-240 and LH20-260 (Fig. S3 (k, l)), the fibrous structures were completely decomposed and disappeared, the heterogeneous fragments were reorganized into coal-like carbon particles, and it showed melted and agglomerated structures.

The fibrous structures in hydrochars are shown in Fig. S4 (b–l). After the HTC process, the surface of fibrous structure became rough, even the LH4-180, which had the lowest SF, showed some wrinkles and cracks on the surface and the original shape of the fibrous structure has been preserved [39, 40]. After that, samples showed different degrees of decomposition depending on the experimental conditions. Overall, with the gradual increase in SF, the surface tended to be rough and decomposed step by step; the tubular

structure as in Fig. S4 (e, f) and skeleton structure as in Fig. S4 (h) inside were revealed and further decomposed. Another manifestation of fibrous structure shrinking was that its diameter was greatly reduced as shown in Fig. S4 (i, j). As shown in Fig. S3 (k, l), when SF were 7.2 and 7.9, respectively, the reaction conditions were sufficiently severe. It caused that the fibrous structure was exhausted and replaced by dense particles after HTC.

The particle size of each sample was measured from SEM pictures using ImageJ software, and plotted as a distribution histogram (Fig. 3). Lavandin was mainly dominated by particles with sizes larger than 100 μm . Because of the degradation during the HTC reaction, a large number of particles smaller than 100 μm appeared in the hydrochars, and this proportion showed a trend of first increasing and then decreasing with the increase in SF. This trend can also be seen from the comparison of SEM images. As the HTC reaction progressed, large particles decomposed into smaller ones, then small particles reorganized and aggregated into larger particles. Finally, when the SF was higher than 7, corresponding to samples LH20-240 and LH20-260, the particle size distribution was similar. A higher temperature could lead to a more uniform average diameter and uniform size distribution [41].

Comparative ATR-FTIR spectra of L and its corresponding hydrochars are shown in Fig. 4. The band at 3600–3000 cm^{-1} is attributed to the O–H stretching vibration in the hydroxyl or carboxyl groups [42]. When SF increased, especially when higher than 7, the intensity of the O–H stretching band decreased significantly, which indicates the results of dehydration and decarboxylation reactions during the HTC. The peaks at 2930 and 2850 cm^{-1} are ascribed to C–H stretching vibration in aromatic and aliphatic structure in L and hydrochars [43]. The

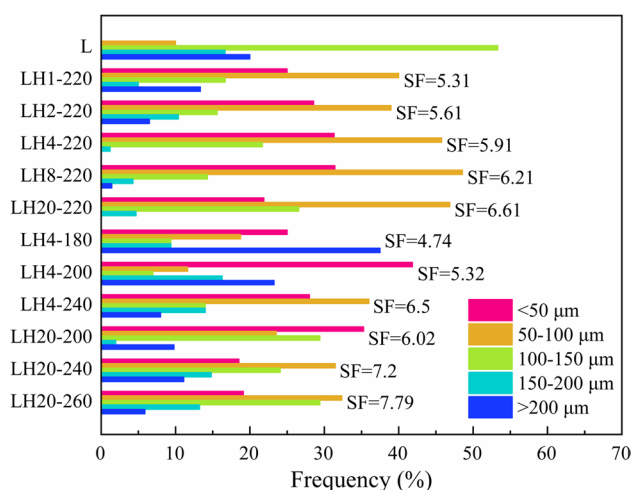
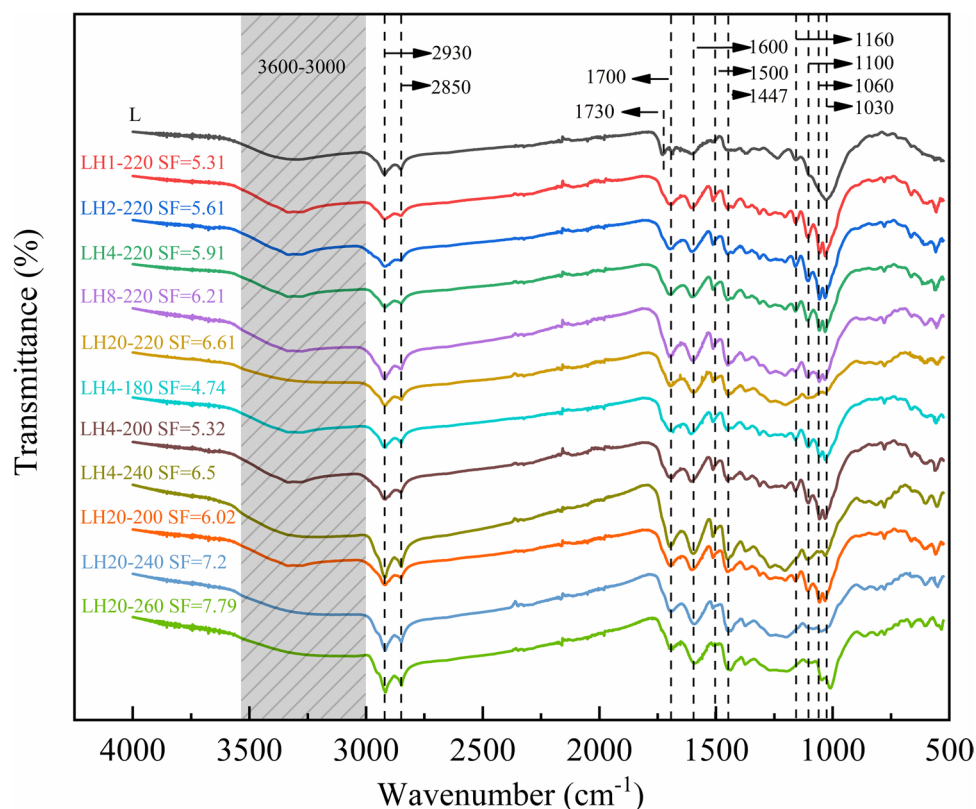


Fig. 3 Statistics of particle size distribution

characteristic C = O stretching of carboxylic acid groups in the hemicellulose appeared approximately at 1730 cm^{-1} in the spectra of L. It disappeared in its corresponding hydrochars due to decomposition of hemicellulose [34, 44]. The peak at around 1700 cm^{-1} in all hydrochar samples is ascribed to the C = O groups in cellulose and lignin. When the temperature increased, relative intensification in this peak occurred due to the disappearance of the band at 1730 cm^{-1} corresponding to the C = O bond

Fig. 4 ATR-FTIR spectra of lavandin and its corresponding hydrochars



in hemicellulose. The intensification points out that the decomposition of hemicellulose occurred at lower temperatures compared with cellulose and lignin [42, 45]. C = C stretching vibration is seen at 1600 and 1500 cm^{-1} and C-H bending vibration is seen at 1447 cm^{-1} , indicating the presence of mononuclear aromatic structures in L and all hydrochars. The aliphatic ether C-O stretching vibration is observable at 1160 , 1100 , 1060 , and 1030 cm^{-1} [40, 46]. Although the exact mechanism of the HTC reactions is still being elucidated, it can still be inferred that dehydration, decarboxylation, and hydrolysis reactions likely occurred during the HTC process.

Combustion Behavior and Thermal Properties of Lavandin and Hydrochars

Thermodegradation of L and hydrochars was performed under constant air flow (150 mL min^{-1}) and constant heating rate (10 °C min^{-1}), in order to evaluate the combustion behavior of the samples. TGA and DTG curves for lavandin (Fig. 5a) and its hydrochars obtained after a short retention time (from 1 to 4 h) (Fig. 5b to d), or a low temperature (below 220 °C) and a relatively short time (4 h) (Fig. 5g and h) depicted the same trend: at around 100 °C water evaporation and devolatilization of low molecular weight component occurred, followed by a first degradation stage between 200 and 400 °C attributed to devolatilization and

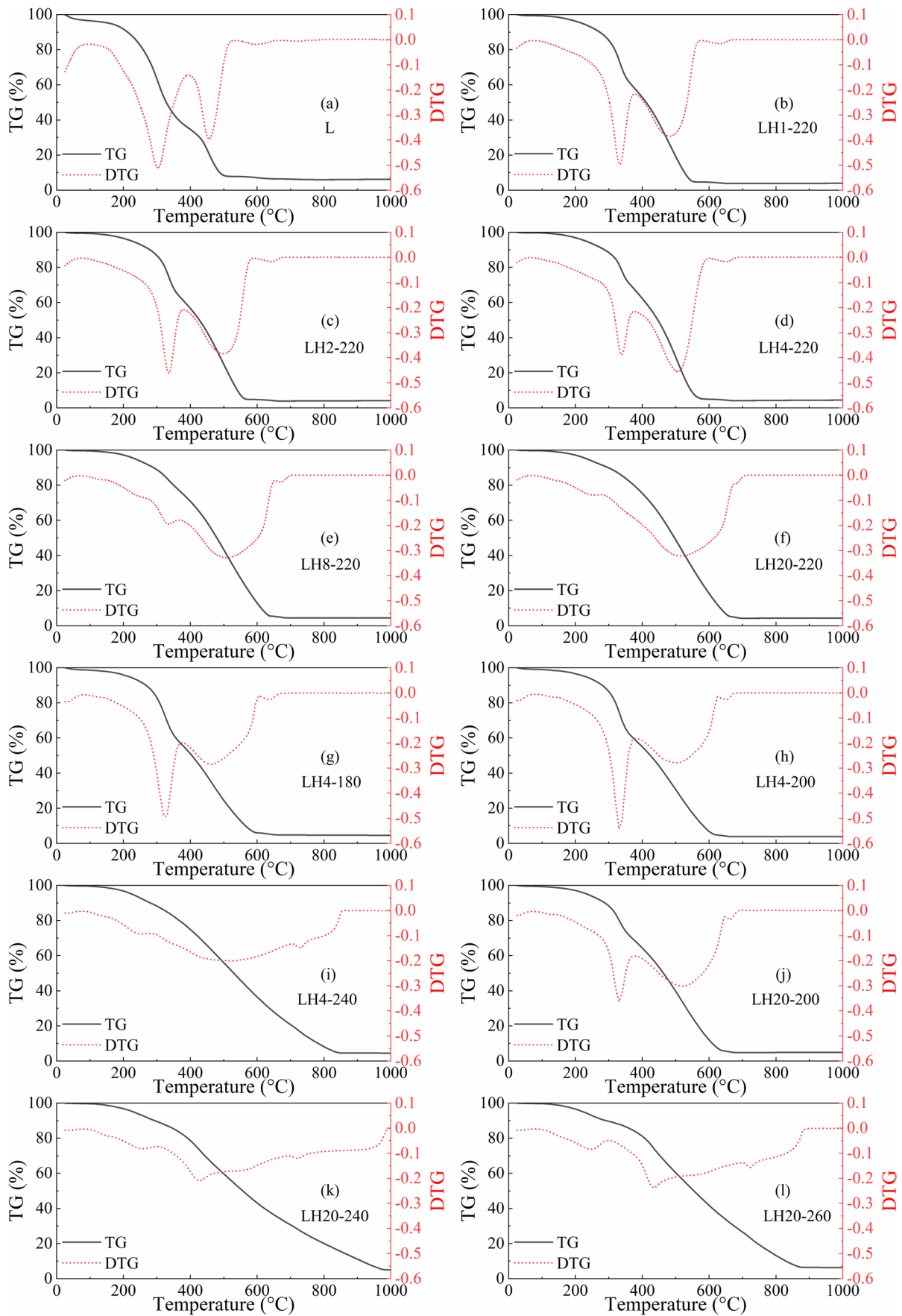


Fig. 5 TGA and DTG curves of thermodegradation under air of a lavandin sample, and its hydrochars: **b** LH1-220, **c** LH2-220, **d** LH4-220, **e** LH8-220, **f** LH20-220, **g** LH4-180, **h** LH4-200, **i** LH4-240, **j** LH20-200, **k** LH20-240, and **l** LH20-260

combustion, and finally a second degradation stage between 400 and 650 °C attributed to char oxidation [28]. Thermodegradation of isolated hemicellulose, cellulose, and lignin has been recently studied [47]. Hemicellulose degradation occurred in a temperature range from 200 to 340 °C. More specifically, a peak and a shoulder were observed at 244 °C and 289 °C, corresponding to fragmentation reactions forming acetic acid and light volatiles, and depolymerization reactions forming furans, respectively. Cellulose degradation was almost complete (0.01% wt of solid residues) and occurred in a narrow temperature range from 300 to 400 °C. Lignin degradation occurred at a very wide temperature range (138–780 °C) due to its abundant aromatic rings with various branches. The maximum weight loss rate was obtained at 254 and 350 °C, corresponding to the decomposition of the polymer structure of the lignin and formation of aromatics hydrocarbons, and phenolics-OH groups, respectively [44]. DTG curves obtained for L LH1-220, LH2-220, LH4-220, LH4-180, and LH4-200 (Fig. 5a to d, g, and h) presented a two-stage degradation process: the first one at 300–400 °C presented a narrow peak with high intensity, and the second one at 400–650 °C presented a broad peak with a moderate intensity. The first degradation stage could be attributed to extractives and hemicellulose degradation, and the second stage could be attributed to cellulose, lignin, and char degradation. Considering that the SF for these hydrochars ranged from 4.74 to 5.91, the various time–temperature combinations chosen for HTC conditions provided the same kind of hydrochar in terms of thermal properties and composition. For $5.91 < SF < 6.5$ (i.e., LH8-220, LH2-220, LH20-200), DTG curves (Fig. 5e, f, j) presented a small and narrow peak between 300 and 400 °C, with a small intensity and a broader one from 400 to 650 °C, with a moderate intensity. The same degradation scenario for $SF < 5.91$ can be proposed, but it is interesting to compare DTG curves obtained in the same temperature condition (i.e., 220 °C and 200 °C, respectively) and discuss about the effect of retention time on hydrochar composition. DTG curves for hydrochars obtained at HTC temperature of 220 °C (Fig. 5b to f) presented the same shape from 1 to 8 h, but the difference resides in peaks intensity and broadness: as the retention time is increased, the intensity of the first peak is decreased until it disappeared when retention time reached 20 h. Broadness of the second peak was increased when retention time was superior to 8 h. Considering that the first peak corresponded to extractive/hemicellulose, at HTC temperature of 220 °C, a retention time superior to 8 h should be applied during HTC for an efficient extractive/hemicellulose

conversion. At HTC temperature of 200 °C (Fig. 5h and j), the first peak intensity strongly decreased between 4 and 20 h but did not disappear, and the broadness on the second peak did not change significantly, meaning that a 20 °C difference in temperature (between 220 and 200 °C) is a more crucial parameter than retention time for biomass thermal conversion. This is confirmed by the observation of DTG curves for hydrochars obtained at constant retention time (20 h) and different HTC temperatures (from 200 to 260 °C) (Fig. 5f, j, k, l), the first peak from DTG curves disappeared as well as the second peak became flatter, when HTC temperature rose from 200 to 220 °C. Regarding hydrochars obtained at SF superior to 6.5 (i.e., LH4-240, LH20-240, LH20-260), the distinction of several degradation stages is not obvious and the thermograms are drastically different from the previous ones (for SF inferior to 6.5). DTG curves (Fig. 5i, k, l) depicted a broad single-stage thermal conversion covering a temperature range from 200 to 800 °C. From these curves, one can conclude that hemicellulose and cellulose were totally degraded during HTC treatment, and lignin was degraded in a lesser extent during HTC treatment. The obtained thermograms corresponded to a large extent to char oxidation. From these three DTG curves, influence of HTC retention time and temperature on hydrochar thermal properties can be examined. At HTC temperature of 240 °C, no significant difference between DTG curves can be observed (Fig. 5i, k), meaning that the retention time selected during HTC has no significant influence on hydrochar properties. At HTC retention time of 20 h (Fig. 5k, l), no significant difference between DTG curves can be observed, meaning that above a certain temperature, retention time has no more influence on hydrochar properties.

Kinetics parameters were calculated from TG/DTG curves, using the CR model and considering order 0.5, 1, and 2 (Table S1). When DTG curves showed two distinct peaks, the kinetics parameters were calculated from the data corresponding to the temperature range of each peak. When DTG curves showed a single broad peak, the kinetics parameters were calculated from the data corresponding to the whole temperature range. Order 1 reaction gave the best fit of experimental results for all hydrochars (R^2 from 0.93 to 0.99); this kinetic order is also in good accordance with similar studies from the literature [39, 40]. Activation energies and pre-exponential factors of order one kinetics are presented for L and hydrochars in Table 3. At constant HTC-retention time (4 h and 20 h), E value decreased with increasing HTC-temperature due to hemicellulose and cellulose degradation (with higher E) during HTC. At constant temperature (220 °C), E values corresponding to the first DTG peak decreased as HTC-retention time increased also due to hemicellulose and cellulose degradation during HTC. E values corresponding to the second DTG peak increased as HTC-retention time increased for hydrochars prepared

in conditions of $SF < 6$. Since the second DTG peak was attributed to lignin and char combustion, it can be concluded that combustion of hydrochars containing a non-negligible fraction of lignin necessitates a higher quantity of energy for oxidation. Hydrochars prepared in conditions of $SF > 6$ have a low E value, meaning that, in these conditions, lignin has been degraded in a large extent during HTC, hydrochar being composed of degradation products (chars). The A values were in the range $185.4 - 0.001 \text{ min}^{-1}$. At constant HTC-temperature ($220 \text{ }^\circ\text{C}$), A values decreased as HTC-retention time increased. At constant HTC-retention time (20 h), A values decreased as HTC-temperature increased. This suggests that the HTC process facilitates the collision frequency related to the combustion process [39]. The highest A values were obtained for the second DTG degradation stage, when DTG curves presented two degradation stages.

T_i and T_b were determined from TG/DTG curves following the intersection and conversion methods, respectively (Table 3). T_i and T_b for L sample ($230 \text{ }^\circ\text{C}$ and $505 \text{ }^\circ\text{C}$, respectively) were lower than T_i and T_b for hydrochars (270 to $330 \text{ }^\circ\text{C}$ and 553 to $950 \text{ }^\circ\text{C}$, respectively), indicating that hydrochars were better biofuels than L. Low T_i means that the volatile matter amount is high. Then, high T_i values indicate that hydrochars used as solid biofuels could be safely stored at ambient temperature and transported without risk of auto-ignition. The highest T_i values corresponded to hydrochars obtained for a retention time superior to 8 h at moderated HTC-temperature ($180\text{--}220 \text{ }^\circ\text{C}$), or at

high HTC-temperatures ($240\text{--}260 \text{ }^\circ\text{C}$). T_b increased as the retention time and/or the HTC-temperature increased. The highest T_b values were obtained at the highest HTC-temperature and the longest retention time ($240\text{--}260 \text{ }^\circ\text{C}$; 20 h). The increase of T_b is correlated with the increase of fixed carbon measured in hydrochars. The longer the retention time during HTC (and/or higher temperature) was, the more thermally stable the carbon components in hydrochars were. Considering T_i and T_b values, the most important parameter of HTC process was retention time, and in a lesser extent temperature. As shown in Table 3, when HTC temperature was $220 \text{ }^\circ\text{C}$, T_i and T_b values increased as retention time increased. When retention time for HTC was 4 h, T_i and T_b values were constant whatever the HTC-temperature in the range $180\text{--}240 \text{ }^\circ\text{C}$.

S values were calculated from the DTG curves and are presented as a function of SF used during HTC experiments in Fig. 6. From this figure, differences in S values clearly appeared as two groups of datasets. The first one, corresponding to S values $1\text{--}1.4 \cdot 10^{-7} \text{ } \%^2 \text{ min}^{-2} \text{ }^\circ\text{C}^{-3}$, has been obtained for hydrochars prepared under HTC conditions with $SF < 5.91$. For these hydrochars, S value was inferior but close to $2 \cdot 10^{-7} \text{ } \%^2 \text{ min}^{-2} \text{ }^\circ\text{C}^{-3}$, indicating a satisfactory general combustion performance. The second group of data, corresponding to S values around $3 \cdot 10^{-8} \text{ } \%^2 \text{ min}^{-2} \text{ }^\circ\text{C}^{-3}$, has been obtained for hydrochars prepared under HTC conditions with $SF > 6$. For these hydrochars, S value was almost tenfold lower than 2

Table 3 Combustion kinetic parameters (E , A , n , R^2) of lavandin (L) and hydrochars (LH) obtained at different temperatures and different retention times. Ignition temperature (T_i), maximum combustion rate temperature (T_m), and burnout temperature (T_b); S : combustibility index $= \frac{\left(\frac{dw}{dt}\right)_{max} \left(\frac{dw}{dt}\right)_{mean}}{T_b \times T_i^2}$, with $\left(\frac{dw}{dt}\right)_{max}$ and $\left(\frac{dw}{dt}\right)_{mean}$ the maximum and mean weight loss rate (%/min), respectively

	SF	Temperature range ($^\circ\text{C}$)	E (kJ/mol)	A (min^{-1})	n	R^2	T_i ($^\circ\text{C}$)	T_b ($^\circ\text{C}$)	S (10^{-8}) ($\%^2 \text{ min}^{-2} \text{ }^\circ\text{C}^{-3}$)
L	NA	160–400	26.43	11.5	1	0.98	230	505	19.8
		400–540	38.46	100.7	1	0.94			
LH1-220	5.31	219–386	34.15	31.0	1	0.97	270	553	13.5
LH2-220	5.61	386–590	43.66	165	1	0.95			
		225–389	33.61	24.3	1	0.97	270	570	12.1
LH4-220	5.91	389–595	43.37	132.8	1	0.94			
		231–384	30.61	10.1	1	0.97	270	582	11.0
LH8-220	6.21	384–610	45.87	185.4	1	0.95			
		235–373	24.15	1.8	1	0.99	312	646	5.25
LH20-220	6.61	373–685	39.22	36.3	1	0.95			
		235–292	18.61	0.4	1	0.99	330	662	4.43
LH4-180	4.74	292–692	32.87	10	1	0.95			
		212–379	33.16	32.3	1	0.98	260	615	11.9
LH4-200	5.32	379–664	30.16	12.3	1	0.98			
		212–379	34.23	34.3	1	0.97	270	615	10.5
LH4-240	6.50	379–664	34.22	24	1	0.93			
		212–782	13.87	0.001	1	0.99	280	821	3.06
LH20-200	6.02	212–517	27.3	8.7	1	0.99	260	880	3.25
LH20-240	7.20	212–940	15.52	0.2	1	0.99	300	950	2.38
LH20-260	7.79	212–782	17.24	0.3	1	0.98	300	851	2.96

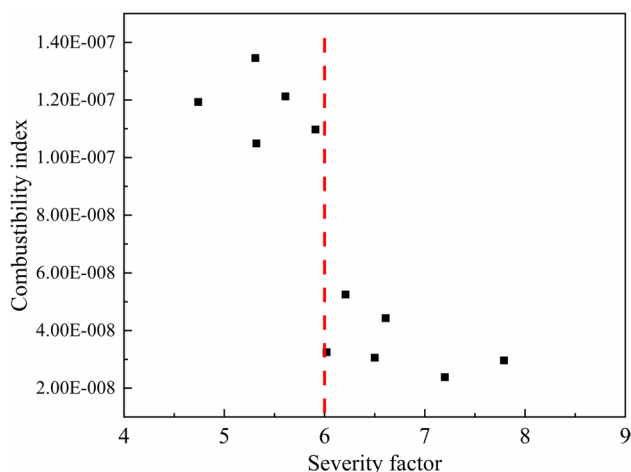


Fig. 6 Combustibility index (S) as a function of severity factor

$10^{-7}\% \text{ min}^{-2} \text{ C}^{-3}$, indicating a bad general combustion performance. Considering HTC conditions, at HTC-temperature of $220\text{ }^{\circ}\text{C}$, S value of hydrochars decreased as retention time increased. Combustibility being linked to VM , the decrease of S could be due to the decrease in VM (approx. 10% reduction) in hydrochars. When HTC-retention time was 20 h, dependency of S value on temperature (from 200 to $260\text{ }^{\circ}\text{C}$) was less noticeable, and from Table 1 variation in VM was inferior to around 5%. The same conclusion can be drawn when HTC-retention time was 4 h and HTC-temperature ranged from 180 to $220\text{ }^{\circ}\text{C}$. Regarding HTC conditions, under HTC-temperature of $220\text{ }^{\circ}\text{C}$, retention time has a great influence on S value, while at high HTC-retention time (20 h) temperature effect is less noticeable on S value. At temperature superior to $220\text{ }^{\circ}\text{C}$, S value was low irrespectively on the HTC-retention time. Hence, combustibility was higher in hydrochars produced at a low temperature. Considering these results, SF is a confident parameter to evaluate combustibility of fuels. In the case of lavandin, hydrochar preparation under SF 6 gave the most interesting combustibility property.

Conclusion

From this study, the following conclusions can be drawn: (i) Lavandin biomass is composed of extractives, hemicellulose, cellulose, and lignin, and combustion occurred between 200 and $550\text{ }^{\circ}\text{C}$; (ii) HTC-temperature was a more influencing parameter on moisture, volatile matter, and fixed carbon, compared to HTC-retention time in biomass conversion during HTC; (iii) when HTC-temperature was above $220\text{ }^{\circ}\text{C}$ and HTC-retention time superior to 4 h (i.e., $SF > 6$), extractives and hemicellulose were totally

converted during HTC treatment, and HHV and hydrochar yield were the highest and hydrochars presented properties close to sub-bituminous coal and lignite; (iv) hydrochars prepared in HTC condition corresponding to $SF < 6$ gave the most interesting combustibility property. An optimal value of $SF = 6$ can be proposed to valorize lavandin biomass into solid fuel through hydrothermal carbonization. Nevertheless, to reach $SF = 6$, it is preferable to use a combination of short HTC-retention time/high HTC-temperature to get a valuable solid fuel.

Supplementary Information The online version contains supplementary material available at <https://doi.org/10.1007/s12155-022-10492-4>.

Acknowledgements Sumeyra Seniha Baran acknowledges Région Sud/Provence-Alpes-Côte d'Azur and the company Jyta for the financial support of her PhD fellowship, as well as Pôle innov'alliance. Xin Li warmly acknowledges China Scholarship Council (CSC) for their support through his PhD fellowship. Professor Pierre-Charles Maria is warmly acknowledged for providing lavandin samples.

Author Contribution Xin Li and Sumeyra Seniha Baran have equally contributed to this work: sample preparation, material characterization, redaction of the manuscript under supervision of Claire Lomenech, Pavel Kuzhir, and Charlotte Hurel. SEM imaging was performed under supervision of François Orange. TGA analysis was performed under supervision of Alice Mija. Elemental analysis was performed by Erik Bonjour and Patrick Jame. All the authors read, commented, corrected the previous versions of the manuscript, and finally approved the final version of the manuscript.

Funding This work received financial support of Région Sud/Provence-Alpes-Côte d'Azur and the company Jyta, China Scholarship Council (CSC) through PhD fellowships. The scanning electron microscope of the Centre Commun de Microscopie Appliquée (CCMA) was funded by the Région Sud/Provence-Alpes-Côte d'Azur and the Conseil Départemental des Alpes Maritimes. This work has also been supported by the French government, through the UCA^{JEDI} Investments in the Future project managed by the National Research Agency (ANR) with the reference number ANR-15-IDEX-01.

Data Availability The datasets generated during the current study are not publicly available due to a confidentiality agreement, but are available from the corresponding author on reasonable request.

Declarations

Competing Interests The authors declare no competing interests.

References

1. Lesage-Meessen L, Bou M, Sigoillot JC, Faulds CB, Lomascolo A (2015) Essential oils and distilled straws of lavender and lavandin: a review of current use and potential application in white biotechnology. *Appl Microbiol Biotechnol*. <https://doi.org/10.1007/s00253-015-6511-7>
2. Saha A, Basak BB (2020) Scope of value addition and utilization of residual biomass from medicinal and aromatic plants. *Ind Crops Prod*. <https://doi.org/10.1016/j.indcrop.2019.111979>

3. Lesage-Meessen L, Bou M, Ginies C, Chevret D, Navarro D, Drula E, Bonnin E, del Rio JC, Odinet E, Bisotto A, Berrin JG, Sigoillot JC, Faulds CB, Lomascolo A (2018) Lavender- and lavender-distilled straws: an untapped feedstock with great potential for the production of high-added value compounds and fungal enzymes. *Biotechnol Biofuels*. <https://doi.org/10.1186/s13068-018-1218-5>
4. Angelova G, Brazkova M, Stefanova P, Blazheva D, Vladev V, Petkova N, Slavov A, Denev P, Karashanova D, Zaharieva R, Enev A, Krastanov A (2021) Waste rose flower and lavender straw biomass—an innovative lignocellulose feedstock for mycelium bio-materials development using newly isolated *Ganoderma resinaceum* GA1M. *J Fungi*. <https://doi.org/10.3390/jof7100866>
5. Greff B, Szigeti J, Varga Á, Lakatos E, Sáhó A, Varga L (2021) Effect of bacterial inoculation on co-composting of lavender (*Lavandula angustifolia* Mill.) waste and cattle manure. *3 Biotech*. <https://doi.org/10.1007/s13205-021-02860-2>
6. Nizamuddin S, Baloch HA, Griffin GJ, Mubarak NM, Bhutto AW, Abro R, Mazari SA, Ali BS (2017) An overview of effect of process parameters on hydrothermal carbonization of biomass. *Renew Sust Energ Rev*. <https://doi.org/10.1016/j.rser.2016.12.122>
7. Kambo HS, Dutta A (2015) A comparative review of biochar and hydrochar in terms of production, physico-chemical properties and applications. *Renew Sust Energ Rev*. <https://doi.org/10.1016/j.rser.2015.01.050>
8. Nawaz A, Kumar P (2022) Elucidating the bioenergy potential of raw, hydrothermally carbonized and torrefied waste *Arundo donax* biomass in terms of physicochemical characterization, kinetic and thermodynamic parameters. *Renew Energ*. <https://doi.org/10.1016/j.renene.2022.01.102>
9. Babinszki B, Jakab E, Sebestyén Z, Blazsó M, Berényi B, Kumar J, Krishna BB, Bhaskar T, Czégény Z (2020) Comparison of hydrothermal carbonization and torrefaction of azolla biomass: analysis of the solid products. *J Anal Appl Pyrolysis*. <https://doi.org/10.1016/j.jaap.2020.104844>
10. Ruiz HA, Conrad M, Sun SN, Sanchez A, Rocha GJ, Romání A, Castro E, Torres A, Rodriguez-Jasso RM, Andrade LP, Smirnova I, Sun RC, Meyer AS (2020) Engineering aspects of hydrothermal pretreatment: from batch to continuous operation, scale-up and pilot reactor under biorefinery concept. *Bioresour Technol*. <https://doi.org/10.1016/j.biortech.2019.122685>
11. Overend RP, Chornet E (1987) Fractionation of lignocelluloses by steam-aqueous pretreatments. *Philos Trans Royal Soc A*. <https://doi.org/10.1098/rsta.1987.0029>
12. Jeder A, Sanchez-Sanchez A, Gadonneix P, Masson E, Ouederni A, Celzard A, Fierro V (2018) The severity factor as a useful tool for producing hydrochars and derived carbon materials. *Environ Sci Pollut Res*. <https://doi.org/10.1007/s11356-017-0366-7>
13. Pauline AL, Joseph K (2020) Hydrothermal carbonization of organic wastes to carbonaceous solid fuel—a review of mechanisms and process parameters. *Fuel*. <https://doi.org/10.1016/j.fuel.2020.118472>
14. Oliveira I, Blöhse D, Ramke HG (2013) Hydrothermal carbonization of agricultural residues. *Biores Technol*. <https://doi.org/10.1016/j.biortech.2013.04.125>
15. Kabakçı SB, Baran SS (2019) Hydrothermal carbonization of various lignocelluloses: fuel characteristics of hydrochars and surface characteristics of activated hydrochars. *Waste Manage*. <https://doi.org/10.1016/j.wasman.2019.09.021>
16. Raheem A, He Q, Ding L, Dastyar W, Yu G (2022) Evaluating performance of pyrolysis and gasification processes of agriculture residues-derived hydrochar: effect of hydrothermal carbonization. *J Clean Prod*. <https://doi.org/10.1016/j.jclepro.2022.130578>
17. Heidari M, Salaudeen S, Dutta A, Acharya B (2018) Effects of process water recycling and particle sizes on hydrothermal carbonization of biomass. *Energy Fuels*. <https://doi.org/10.1021/acs.energyfuels.8b02684>
18. Chen SF, Mowery RA, Chambliss CK, van Walsum GP (2007) Pseudo reaction kinetics of organic degradation products in dilute-acid-catalyzed corn stover pretreatment hydrolysates. *Biotechnol Bioeng*. <https://doi.org/10.1002/bit.21480>
19. American Society for Testing and Materials (2013) American Society for Testing and Materials (ASTM). E871–82. <https://www.astm.org/e0871-82r19.html>. <https://doi.org/10.1520/E0871-82R19>
20. American Society for Testing and Materials (2015) American Society for Testing and Materials (ASTM). E1755–01. <https://www.astm.org/e1755-01.html>. <https://doi.org/10.1520/E1755-01>
21. American Society for Testing and Materials (2013) American Society for Testing and Materials (ASTM). E872–82. <https://www.astm.org/e0872-82r19.html>. <https://doi.org/10.1520/E0872-82R19>
22. Channiwala SA, Parikh PP (2002) A unified correlation for estimating HHV of solid, liquid and gaseous fuels. *Fuel*. [https://doi.org/10.1016/S0016-2361\(01\)00131-4](https://doi.org/10.1016/S0016-2361(01)00131-4)
23. American Society for Testing and Materials (2016) American Society for Testing and Materials (ASTM). E1690–08. <https://www.astm.org/standards/e1690>. <https://doi.org/10.1520/E1690-08R21>
24. TAPPI (2006) Acid-insoluble lignin in wood and pulp (reaffirmation of T 222 Om-02). Chemical Properties (New York Technical association of the pulp and paper industry). <https://www.tappi.org/content/SARG/T222.pdf>
25. Schneider CA, Rasband WS, Eliceiri KW (2012) NIH Image to ImageJ: 25 years of image analysis. *Nat Methods*. <https://doi.org/10.1038/nmeth.2089>
26. Neeft JP, Hoornaert F, Makkee M, Moulijn JA (1996) The effects of heat and mass transfer in thermogravimetric analysis. A case study towards the catalytic oxidation of soot. *Thermochim Acta*. [https://doi.org/10.1016/S0040-6031\(96\)03002-X](https://doi.org/10.1016/S0040-6031(96)03002-X)
27. Lu JJ, Chen WH (2015) Investigation on the ignition and burnout temperatures of bamboo and sugarcane bagasse by thermogravimetric analysis. *Appl Energy*. <https://doi.org/10.1016/j.apenergy.2015.09.026>
28. Liu Z, Quek A, Hoekman SK, Balasubramanian R (2013) Production of solid biochar fuel from waste biomass by hydrothermal carbonization. *Fuel*. <https://doi.org/10.1016/j.fuel.2012.07.069>
29. Peng C, Zhai Y, Zhu Y, Xu B, Wang T, Li C, Zeng G (2016) Production of char from sewage sludge employing hydrothermal carbonization: char properties, combustion behavior and thermal characteristics. *Fuel*. <https://doi.org/10.1016/j.fuel.2016.02.068>
30. Coats AW, Redfern JP (1964) Kinetic parameters from thermogravimetric data. *Nature*. <https://doi.org/10.1038/201068a0>
31. Islam MA, Kabir G, Asif M, Hameed BH (2015) Combustion kinetics of hydrochar produced from hydrothermal carbonisation of Karanj (*Pongamia pinnata*) fruit hulls via thermogravimetric analysis. *Biores Technol*. <https://doi.org/10.1016/j.biortech.2015.06.094>
32. Santana MS, Alves RP, da Silva Borges WM, Francisquini E, Guerreiro MC (2020) Hydrochar production from defective coffee beans by hydrothermal carbonization. *Biores Technol*. <https://doi.org/10.1016/j.biortech.2019.122653>
33. Samuelsson R, Burvall J, Jirjis R (2006) Comparison of different methods for the determination of moisture content in biomass. *Biomass Bioenerg*. <https://doi.org/10.1016/j.biombioe.2006.06.004>
34. Nakason K, Panyapinyopol B, Kanokkantapong V, Viriya-empikul N, Kraithong W, Pavasant P (2018) Hydrothermal carbonization of unwanted biomass materials: effect of process temperature and retention time on hydrochar and liquid fraction. *J Energy Inst*. <https://doi.org/10.1016/j.joei.2017.05.002>

35. Park KY, Lee K, Kim D (2018) Characterized hydrochar of algal biomass for producing solid fuel through hydrothermal carbonization. *Biores Technol.* <https://doi.org/10.1016/j.biortech.2018.03.003>
36. Sharma HB, Sarmah AK, Dubey B (2020) Hydrothermal carbonization of renewable waste biomass for solid biofuel production: a discussion on process mechanism, the influence of process parameters, environmental performance and fuel properties of hydrochar. *Renew Sust Energy Rev.* <https://doi.org/10.1016/j.rser.2020.109761>
37. Cai J, Li B, Chen C, Wang J, Zhao M, Zhang K (2016) Hydrothermal carbonization of tobacco stalk for fuel application. *Biores Technol.* <https://doi.org/10.1016/j.biortech.2016.08.098>
38. Guo S, Dong X, Wu T, Shi F, Zhu C (2015) Characteristic evolution of hydrochar from hydrothermal carbonization of corn stalk. *J Anal Appl Pyrolysis.* <https://doi.org/10.1016/j.jaap.2015.10.015>
39. Khan T, Saud A, Jamari S, Rahim M, Park J, Kim H (2019) Hydrothermal carbonization of lignocellulosic biomass for carbon rich material preparation: a review. *Biomass Bioenerg.* <https://doi.org/10.1016/j.biombioe.2019.105384>
40. Guardia L, Suárez L, Querejeta N, Pevida C, Centeno T (2018) Winery wastes as precursors of sustainable porous carbons for environmental applications. *J Clean Prod.* <https://doi.org/10.1016/j.jclepro.2018.05.085>
41. Falco C, Baccile N, Titirici M (2011) Morphological and structural differences between glucose, cellulose and lignocellulosic biomass derived hydrothermal carbons. *Green Chem.* <https://doi.org/10.1039/C1GC15742F>
42. Lin Y, Ma X, Peng X, Yu Z (2016) A mechanism study on hydrothermal carbonization of waste textile. *Energy Fuels.* <https://doi.org/10.1021/acs.energyfuels.6b01365>
43. Gao P, Zhou Y, Meng F, Zhang Y, Liu Z, Zhang W, Xue G (2016) Preparation and characterization of hydrochar from waste eucalyptus bark by hydrothermal carbonization. *Energy.* <https://doi.org/10.1016/j.energy.2015.12.123>
44. Petrović J, Perišić N, Maksimović J, Maksimović V, Kragović M, Stojanović M, Laušević M, Mihajlović M (2016) Hydrothermal conversion of grape pomace: detailed characterization of obtained hydrochar and liquid phase. *J Anal Appl Pyrolysis.* <https://doi.org/10.1016/j.jaap.2016.02.010>
45. Kabakcı S (2019) Pyrolysis and combustion characteristics and kinetics of wood sawdust and wood sawdust hydrochar. *Environ Prog Sustain Energy.* <https://doi.org/10.1002/ep.13315>
46. Zhu G, Yang L, Gao Y, Xu J, Chen H, Zhu Y, Wang Y, Liao C, Lu C, Zhu C (2019) Characterization and pelletization of cotton stalk hydrochar from HTC and combustion kinetics of hydrochar pellets by TGA. *Fuel.* <https://doi.org/10.1016/j.fuel.2019.02.039>
47. Chen WH, Wang CW, Ong HC, Show PL, Hsieh TH (2019) Torrefaction, pyrolysis and two-stage thermodegradation of hemicellulose, cellulose and lignin. *Fuel.* <https://doi.org/10.1016/j.fuel.2019.116168>

Publisher's Note Springer Nature remains neutral with regard to jurisdictional claims in published maps and institutional affiliations.